Thermal Degradation Chemistry of Alkyl Quaternary Ammonium Montmorillonite

Wei Xie,[†] Zongming Gao,[†] Wei-Ping Pan,*[,†] Doug Hunter,[‡] Anant Singh,[§] and Richard Vaia*[,||]

Thermal Analysis Laboratory, Material Characterization Center, Department of Chemistry, Western Kentucky University, Bowling Green, Kentucky 42101; Southern Clay Products, Inc., 1212 Church Street, Gonzales, Texas 78629; Triton Systems, Inc., 200 Turnpike Road, Chelmsford, Massachusetts 01824; and AFRL/MLBP, BLDG 654, 2941 P Street, Wright-Patterson AFB, Ohio 45433

Received April 4, 2001. Revised Manuscript Received June 25, 2001

The thermal stability of organically modified layered silicate (OLS) plays a key role in the synthesis and processing of polymer-layered silicate (PLS) nanocomposites. The nonoxidative thermal degradation of montmorillonite and alkyl quaternary ammonium-modified montmorillonite were examined using conventional and high-resolution TGA combined with Fourier transform infrared spectroscopy and mass spectrometry (TG−FTIR−MS) and pyrolysis/GC−MS. The onset temperature of decomposition of these OLSs was approximately 155 °C via TGA and 180 °C via TGA−MS, where TGA−MS enables the differentiation of water desorbtion from true organic decomposition. Analysis of products (GC−MS) indicates that the initial degradation of the surfactant in the OLS follows a Hoffmann elimination reaction and that the architecture (trimethyl or dimethyl), chain length, surfactant mixture, exchanged ratio, or preconditioning (washing) does not alter the initial onset temperatures. Catalytic sites on the aluminosilicate layer reduce thermal stability of a fraction of the surfactants by an average of 15−25 °C relative to the parent alkyl quaternary ammonium salt. Finally, the release of organic compounds from the OLS is staged and is associated with retardation of product transfer arising from the morphology of the OLS. These observations have implications to understanding the factors impacting the interfacial strength between polymer and silicate and the subsequent impact on mechanical properties as well as clarifying the role (advantageous or detrimental) of the decomposition products in the fundamental thermodynamic and kinetic aspects of polymer melt intercalation.

Introduction

Inorganic particles, such as talc, mica, carbon black, and fused silica, are widely used as reinforcement additives for polymers. At present, polymers reinforced by low weight percentages (1−10 wt %) of nanoscopically dispersed organically modified layered silicates (OLS) are attracting the attention of government, academic, and industrial researchers because of the unprecedented suite of new and enhanced properties relative to the unfilled resin. These polymer-layered silicate (PLS) nanocomposites can attain a degree of stiffness and strength with substantially less inorganic content than comparable glass- or mineral-reinforced polymers. Furthermore, the nanoscopic phase distribution result in additional properties, such as flame retardency, enhanced barrier properties, and ablation resistance, which are not observed in either component.[1]

The layered silicates (alternatively referred to as clay minerals[2]) possess the same structural characteristics as the well-known minerals talc and mica and are comprised of stacks of hydrated aluminosilicate. Their crystal structure consists of two-dimensional layers (thickness ∼ 0.96 nm) formed by fusing two silica tetrahedral sheets with an edge-shared octahedral sheet of either alumina or magnesia.[3,4] Stacking of these layers leads to van der Waals gaps or galleries. The galleries (alternatively referred to as interlayers) are occupied by cations, typically Na^+ and/or Ca^{2+}, which balance the charge deficiency that is generated by isomorphous substitution within the layers (e.g., tetrahedral Si^{4+} by Al^{3+} or octahedral Al^{3+} by Mg^{2+}). Variation in the amount, type, and crystallographic origin of the excess layer charge results in a large family of natural (e.g., montmorillonite, hectorite, saponite) and synthetic (e.g,. Laponite, fluorohectorite) layered silicates exhibiting different physical and chemical char-

[†] Western Kentucky University.
[‡] Southern Clay Products, Inc.
[§] Triton Systems, Inc.
[||] AFRL/MLBP.

(1) Giannelis, E. P. *Adv. Mater.* **1996**, *8* (1), 29. Alexandre, M.; Dubois, P. *Mater. Sci. Eng.* **2000**, *28*, 1−63. *Polymer-Clay Nanocomposites*, Pinniavaia, T., Beal, G. W., Eds. John Wiley and Sons: New York, 2000.

(2) In the nanocomposite literature, the term clay is increasingly used synonymously for layered silicates. Note though that clay is traditionally used to refer to any mineralogical deposit with particle size less than 0.2 μm. More correctly, the layered silicates conventionally utilized for polymer nanocomposites are clay minerals or 2:1 phyllosilicates.

(3) Ciullo, P. A., *CHIMICA OGGI/chem. today*, March/April **1997**.

(4) Brindely, G. W.; Brown, G. *Crystal Structure of Clay Minerals and their X-ray Identification*; Mineralogical Society: London, 1980.

10.1021/cm010305s CCC: $20.00
Published on Web 08/11/2001

acteristics, such as layer size, stacking perfection, reactivity, and Lewis acidity. To enhance compatibility with organophillic polymers for PLSs, the interlayer cations are replaced with organic ammonium and phosphonium cations, functionalizing the aluminosilicate surface. Depending on the functionality, packing density, and length of these modifiers, the organically modified layered silicate (OLS) may be engineered to optimize compatibility with a given polymer.

In contrast to the recent emergence of layered silicates as nanoscale reinforcing agents for commodity plastics, natural and synthetic clay minerals have been used for more then 40 years as catalysts and catalytic supports for organic reactions.[5,6] The complex crystallographic structure and habit of clay minerals results in a diverse range of catalytic activity at both the layer edge and, to a lesser extent, the planer siloxane surface.[7] The fraction of total surface area of an individual layer associated with the edge is 2−4% for layers with radii between 50 and 25 nm, respectively. Weakly acidic SiOH and strongly acidic bridging hydroxyl groups present at the edge act as Bronsted acid sites. Lewis acid centers can arise at the layer edge from partially coordinated metal atoms, such as Al^{3+}, or along the siloxane surface from isomorphic substitution of multivalent species, such as Fe^{2+} and Fe^{3+}, and crystallographic defect sites within the layer. These Lewis acid sites can accept single electrons from donor molecules with low ionization potential, coordinate organic radicals, or abstract electrons from vinylic monomers. In addition to direct catalytic activity, the morphology and degree of aggregation impact the rate of product and reactant transfer within the pseudo-two-dimensional galleries, greatly modifying the kinetics of reactions. Unfortunately, minimal studies connecting the chemical reactivity of the parent aluminosilicate to the stability of the organic modifiers or polymers within the OLS and PLS nanocomposites are available.

When preparing PLS nanocomposites, elevated temperatures are required for fabrication via melt intercalation and, irrespective of the fabrication route (solution mediated, in situ polymerization or melt intercalation), for bulk processing. If the processing temperature is greater than the thermal stability of the organic treatment on the OLS, decomposition will occur, altering the interface between the filler and polymer. Quantification of the onset temperature of degradation, resultant products, and subsequent influence on the stability of the polymer host is critical. Furthermore, previous and current fundamental experimental and theoretical investigations of the thermodynamics[7] and kinetics[8] of hybrid formation as well as the subsequent relaxation behavior of confined chains[9] implicitly assume the thermal stability of the OLS, i.e., the idealized surfactant modified aluminosilicate surface is maintained through-out elevated temperature excursions. Unfortunately, minimal investigations are available that systematically determine the thermal stability of the OLS, establish the degradation mechanisms, examine the various factors influencing the stability, or ascertain the associated effect on the OLS−polymer interface.

To begin to understand the thermal stability and degradation mechanisms of organically modified layered silicates, the stability, fine structure, and evolution of gaseous species from alkyl quaternary ammonium montmorillonites are investigated in-depth with conventional thermogravemetric analysis (TGA) and high-resolution TGA, TGA combined with Fourier transform infrared spectroscopy (FTIR), mass spectrometry (TG−FTIR−MS), and pyrolysis/GC−MS and in situ X-ray diffraction. Briefly, this article will discuss (1) the temperature regimes of thermal degradation reactions within alkyl quaternary ammonium montmorillonite and natural montmorillonite, (2) the onset temperatures, stages, and products of organic decomposition within OLSs, (3) structural changes to the OLS during the initial stages of organic decomposition, and (4) the mechanism and pathways of organic decomposition for OLSs. These studies provide the foundation for subsequent investigations of the influences of the various inorganic (e.g., mineral, isomorphic substitution, crystal habit, layer charge density) and organic (surfactant architecture, chemical composition, omium type, covalent attachment) factors on the thermal−oxidative stability of the OLS and PLS nanocomposites.

Experimental Section

Materials. Six alkyl quaternary ammonium chlorides ($R_3R'N^+Cl$ and $R_2R'_2N^+Cl$, used as received from Akzo Nobel Chemicals, Inc.) were utilized to fabricate various OLS from a base Na^+ montmorillonite (Cloisite Na^+, cation exchange capacity, CEC = 92 mequiv/100 g, mean formula unit $Na_{0.65}[Al,Fe]_4Si_8O_{20}(OH)_2$, Southern Clay Products, Inc.). The alkyl quaternary ammonium surfactants, mean molecular weight, milliequivalent exchange ratio (MER), intended organic content, and interlayer distance (d_{001}) of the OLSs are detailed in Table 1. Coco, tallow, and hydrogenated tallow quaternary ammonium surfactants are derived from natural products and are commonly utilized in commercial OLSs. They consist of a mixture of quaternary ammonium salts with various lengths of saturated and unsaturated alkyl chains. The nominal compositions of these natural products are summarized in Table 2.[10]

The organically modified montmorillonites were prepared using commercial processes (Southern Clay Products, Inc) that parallel conventional literature procedures.[11] Briefly, quaternary ammonium salt is added to a purified montmorillonite slurry, and the flocculated product is removed by filtration, dried, and milled. LOI (loss on ignition) results suggest that less than 5% unexchanged quaternary surfactant is present at the standard exchange level (MER = 95 mequiv/100 g of

(5) Solomon, D. H.; Hawthorne, D. G. *Chemistry of Pigments and Fillers*; Krieger, Malabar, FL, 1991.

(6) Sposito, G.; Skipper, N. T.; Sutton, R.; Park, S.-H.; Soper, A. K.; Greathouse, J. A. *Proc. Natl. Acad. Sci. U.S.A.* **1999**, *96*, 3358. Sherman, J. D. *Proc. Natl. Acad. Sci. U.S.A.* **1999**, *96*, 3471.

(7) Vaia, R. A.; Giannelis, E. P. *Macromoleules* **1997**, *30*, 7990. Vaia, R. A.; Giannelis, E. P. *Macromoleules* **1997**, *30*, 8000. Ginzburg, V. V.; Balazs, A. C. *Macromoleules* **1999**, **32**, 5681. Lyatskaya, Y.; Balazs, A. C. *Macromoleules* **1998**, *31*, 6676. V. V. Ginzburg, C. Singh, A. C. Balazs, *Macromoleules* **2000**, *33*, 1089. Balazs, A. C.; Singh, C.; Zhulina, E.; Lyatskaya, Y. *Acc. Chem. Res* **1999**, *32*, 651.

(8) Vaia, R. A.; Jandt, K. D.; Kramer, E. J.; Giannelis, E. P. *Macromol.* **1995**, *28*, 808. Manias, E.; Chen, H.; Krishnamoorti, R.; Genzer, J.; Kramer, E. J.; Giannelis, E. P. *Macromoleules* In press. Lee, J. Y.; Baljon, R. C.; Loring, R. F.; Panagiotopoulos, A. Z. *J. Chem. Phys.* **1998**, *109*, 10321. Lee, J. Y.; Baljon, R. C.; Loring, R. F *J. Chem. Phys* **1999**, *111*, 9754. Baljon, R.; Lee, J. Y.; Loring, R *J. Chem. Phys.* **1999**, *111*, 9068.

(9) Giannelis, E. P.; Krishnamorti, R.; Manias, E. *Adv. Polym. Sci.*, **1999**, *138*, 108. Krishnamorti, R.; Vaia, R. A.; Giannelis, E. P. *Chem. Mater.* **1996**, *8*, 1728.

(10) Akzo Nobel Chemicals, Inc, product literature.

(11) Vaia, R. A.; Teukolsky, R. K.; Giannelis, E. P. *Chem. Mater.* **1994**, *6*, 1017−1022.

Table 1. Alkyl Quaternary Ammonium Modified Montmorillonites

	surfactant[a]	surfactant molecular wt (g/mol)	milliequivalent exchange ratio, MER (mequiv/100 g)	fraction organic content	d_{001} (nm)
2044	TMC	238.6	95	0.185	1.44
2046	TMT	301.7	95	0.223	1.80
2047	TMD	228.5	95	0.178	1.50
2048	TMO	312.7	95	0.229	1.82
2423	DMDC	403.0	95	0.277	1.86
2427	DMDHT	529.3	140	0.426	3.48
2428	DMDHT	529.3	125	0.388	3.25
2429	DMDHT	529.3	95	0.335	2.60

[a] TMC, trimethyl-coco-ammonium chloride; TMT, trimethyl-tallow-ammonium chloride; TMD, trimethyldodecylammonium chloride; TMO, trimethyloctadecylammonium chloride; DMDC, dimethyl-dicoco-ammonium chloride; DMDHT, dimethyl-dihydrogenated tallow-ammonium chloride.

Table 2. Percent Composition of Natural Product Alkyls[10]

	n[a]	coco $\bar{n}$[b] = 12.72	tallow $\bar{n}$ = 17.22	hydrogenated tallow $\bar{n}$ = 17.22
saturated	8	6		
	10	7		
	12	51		
	14	19	3	3.5
	15		0.5	0.5
	16	9	29	31
	17		1	1
	18	2	20	61
unsaturated	14′		0.5	
	16′	6	2	
	18′		44	3

[a] n: number of carbon atoms per alkyl chain. [b] $\bar{n}$: mean number of carbons per chain.

montmorillonite) generally used in this study. In some instances, subsequent washing of the OLSs consisted of slurring the exchanged montmorillonite in methanol, decanting, and repeating for a total of three washings or refluxing ethanol through a Soxhlet containing the OLS for 3−9 h. The final organic content after washing with methanol corresponded to the CEC of the montmorillonite (see Table 4 below). However, Soxhlet extraction of 2044 resulted in an organic content ∼15% lower than CEC. This implies that the original exchange reaction was not complete (a fraction of Na^+ still remained within the interlayer) or that the washing procedure introduced a fraction of acidic protons that reduced the effective CEC of the aluminosilicate.[12]

Thermal Characterization. Thermogravimetric analysis (conventional and high resolution) was conducted on a TA Instruments TGA2950 using an ultrahigh purity (UHP) nitrogen atmosphere, with heating from room temperature to 1000 °C (2 °C/min for conventional TGA). High-resolution TGA differs from conventional TGA in that the heating rate is coupled to mass loss such that the sample temperature is not raised until the gaseous evolution at a particular temperature is completed. TGAs were calibrated with indium, tin, zinc, and silver (2 °C/min from T_m − 100 °C to T_m + 50 °C; the melting point was determined from dT/dt (T)). The standard error, σ, for T_{onset} and T_{max} is 1.5 and 1 °C, respectively. The total fraction of organic in the OLS was determined by adjusting the total mass loss from 150 to 1000 °C with the mass loss of the parent Na^+montmorillonite from 450 to 700 °C (5.48%) to account for the mass loss associated with dehydroxylation of the aluminosilicate. These values agreed with those determined from loss on ignition determined for selected samples.

FTIR spectra of samples in pressed KBr pellets were recorded on a Perkin-Elmer 1600 series infrared spectrometer.

(12) Pinniavaia, T. J. *Chem. Mater.* **2001**, submitted.

Table 3. Decomposition Temperatures in Ultra-pure N_2

	TGA, °C				MS °C	
	$T_{onset,1}$	$T_{max,1}$	$T_{onset,2}$	$T_{max,2}$	$T_{onset,1}$	$T_{onset,2}$
			Trimethylalkyl			
2044	151 (120[c])	226	263 (258[c])	383	167	252
2044a[a]	163	232	249	378		
2044b[a]	177	235	246	382		
2044c[a]	178	—[d]	—[d]	383		
2046	150 (139[c])	226	262 (263[c])	375	177	268
2047	151 (128[c])	224	258 (259[c])	384	178	258
2048	143 (135[c])	223	259 (260[c])	368	164	244
TMC	177	241				
TMT	179	238				
TMD	181	245				
TMO	187	242				
			Dimethyldialkyl			
2423	137	238	262	291, 366[e]		
2427	157	242	260	300, 388[e]		
2428	155	247	255	301, 370[e]		
2428a[b]	160	—[d]	—[d]	293, 349[e]		
2429	154	231	243	277, 344[e]		
2429a[b]	161	—[d]	—[d]	293, 348[e]		

[a] Soxhlet extract with ethanol for (a) 3 h, (b) 6 h, and (c) 9 h. [b] Three-time washing with methanol. [c] Onset temperature determined before predrying OLS at 140 °C. [d] Magnitude of initial event too small to allow estimation of temperature. [e] Second decomposition peaks.

Table 4. Relative Mass Loss (TGA) during Decomposition of the OLS

	% mass loss			% total organic[b]	fraction organic evolved in 1st event
	<120 °C	120−450 °C	1st event[a]		
			Trimethylalkyl		
2044	0.90	17.6	4.9	19.00	0.26
2044a[c]	0.63	13.0	1.6	15.60	0.12
2044b[c]	0.50	14.1	1.0	15.08	0.07
2044c[c]	0.61	14.2	0.7	15.09	0.05
2046	0.78	23.0	8.0	23.93	0.33
2047	1.19	17.8	4.8	19.16	0.25
2048	1.64	23.7	9.0	23.88	0.38
			Dimethyldialkyl		
2423	0.33	24.7	7.4	26.00	0.28
2427	0.60	40.0	7.7	41.52	0.19
2428	0.57	38.8	4.0	38.85	0.10
2428a[d]	0.48	32.1	0.3	32.06	0.01
2429	0.72	31.9	2.6	32.77	0.08
2429a[d]	0.49	31.3	0.3	31.66	0.01

[a] First organic decomposition event corresponds to mass loss between $T_{onset,1}$ and $T_{onset,2}$. [b] Percent total organic corresponds to the mass loss between $T_{onset,1}$ and 1000 °C, corrected with regard to the appropriate mass fraction of montmorillonite in the OLS for the mass loss associated with dehydroxylation of the montmorillonite lattice [% mass loss, pristine montmorillonite (450−750°C) = 5.48%]. [c] Soxhlet extract with ethanol for (a) 3 h, (b) 6 h, (c) 9 h. [d] Three-time washing with methanol.

The IR detection range was 450−4500 cm^{-1} with a resolution of 4 cm^{-1}. TG−FTIR experiments are conducted on a DuPont 951 TGA interfaced to a Perkin-Elmer 1600 series FTIR with a permanent 1-in. silicon transfer line. The purge gas carries the decomposition products from the TGA through a 70-mL sample cell with KBr crystal windows. For detection of the decomposition products, the cell was placed in the IR scanning path and kept at 150 °C by wrapping with heating tape to prevent possible condensation.

TG−MS experiments were conducted on an SDT (Simultaneous TGA&DTA) 2960 (2 °C/min) interfaced to a Fisons VG Thermolab mass spectrometer by means of a heated capillary transfer line. The Fisons unit is based on a quadrupole design with a 1−300 atomic mass units (amu) mass range. The sample gas from the interface was ionized at 70 eV. The system operates at a pressure of 1 × 10^{-6} Torr. A NIST library database was used for MS analysis. Pyrolysis/GC−MS experi-

ments were carried out on a Pegasus II GC−MS system, which includes a time-of-flight mass spectrometer and a high-speed gas chromatograph.

Morphological Characterization. Standard wide-angle X-ray diffraction data was collected in reflection on powders using a Scintag XDS2000 diffractometer with Cu Kα radiation at 1°/min. In situ small-angle X-ray scattering (SAXS) experiments were conducted at the Advanced Polymers Beamline (X27C) of the National Synchrotron Light Source (NSLS), Brookhaven National Laboratory (BNL). The wavelength of the incident X-rays was 0.1307 nm defined by a double multilayer monochromator. The synchrotron X-rays were collimated to 600 μm using a three-pinhole collimator.[13] Data were collected using a Braun linear position sensitive detector[14] at 1.475 m. The scattering angle was calibrated using silver behenate. Constant heating rate measurements (5 °C/min, 40−280 °C) were carried out on pressed powder samples mounted in a copper holder, within an oven with N_2 purge and aligned within the beam. Data acquisition times were 30 s per scan, yielding a temperature averaging of 2.5 °C per scan. All the X-ray data was corrected for beam fluctuations and sample absorption. Peak position and breadth (full width at half-maximum, fwhm) were determined by fitting the data in the region of the basal reflection to a Lorentzen function using a nonlinear least-squares fitting algorithm (Genplot, v 2.02).

Results

In general, thermal degradation of these nanoscale organic−inorganic hybrid materials is a complex process. Initially, to qualify the organic decomposition processes, the general characteristics of pristine Na^+ montmorillonite and a representative alkyl quaternary ammonium montmorillonite will be compared. Next, procedures to define the onset of organic decomposition will be developed and utilized to discuss the effect of molecular architecture of the quaternary surfactant on the onset of degradation. Finally, details of the thermal decomposition process, degradation products and relation to changes in the layered silicate morphology during decomposition will be considered.

Characteristics of Decomposition. DTG (derivative thermogravimetry) curves of pristine montmorillonite and a typical alkyl quaternary ammonium montmorillonite (2044) are shown in Figure 1, parts a and b. The high-resolution (HR) DTG data further differentiate the various overlapping events. Note that because high-resolution TGA uses varying heating rates and effectively an isothermal hold at a mass-loss event, decomposition temperatures, as defined by the peak in the DTG curve, will be lower than observed in conventional TGA.

Decomposition of pristine montmorillonite corresponds to previous reports, which generally identify two regions below 1000 °C.[15] Free (absorbed) water residing between montmorillonite crystallites and interlayer water residing between the aluminosilicate layers and comprising the hydration spheres of the cations evolve between 100 and 400 °C.[4,15−16] Between 500 and 1000 °C, dehydroxylation of the aluminosilicate lattice occurs.

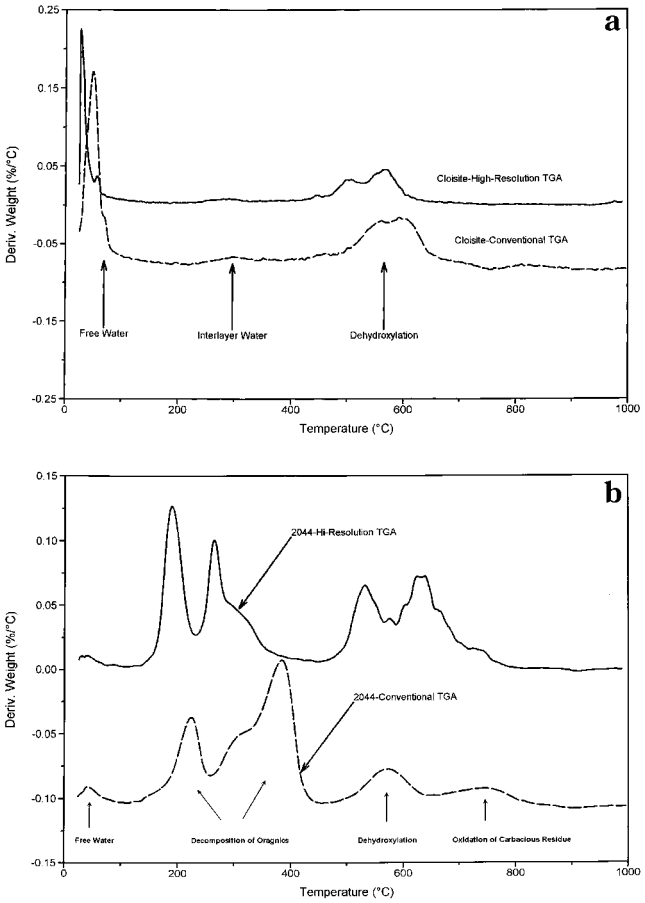

Figure 1. DTG (derivative weight loss) curves from conventional and high-resolution TGA of (a) pristine montmorillonite and (b) a representative alkyl quaternary ammonium montmorillonite (2044).

In conjunction, the crystal structure has been observed to initially transform into spinel, cristobolite, mullite, and/or pyroxenes (enstatite).[16] At temperatures greater than 1300 °C, mullite, cristobolite, and cordierite form and subsequently melt at temperatures in excess of 1500 °C (mullite, 1850 °C; pure cristobolite, 1728 °C; and cordierite, ∼1550 °C).[17]

Thermal decomposition of the OLSs is conveniently considered in four regions. Briefly, evolution of absorbed water and gaseous species occurs below 180 °C (region I). Organic substances evolve from 200 to 500 °C (region II). Dehydroxylation of the aluminosilicate occurs from 500 to 700 °C (region III) and evolution of products associated with residual organic carbonaceous residue occurs between 700 and 1000 °C (region IV). Although conventional PLS service environment would not include the temperatures in regions III and IV, the complete degradation behavior of the OLS at these extreme temperatures has implications for the utilization of exfoliated OLSs as flame-retardant and ablation additives.

For both the organic-modified montmorillonite (2044) and the sodium montmorillonite (cloisite Na^+), the initial mass loss is dominated by water. For closite Na^+, release of water begins around 40 °C, peaks at 62 °C, and continues till about 300 °C. The HR-DTG curve

(13) Hsiao, B. S.; Gardner, K. H.; Wu, D. Q.; Chu, B. *Polymer* **1988**, *29*, 1745.
(14) Rapp, G.; Gabriel, A.; Dosiere, M.; Kock, M. H. J. *Nucl. Inst., Methods Phys. Res. A.* **1995**, *357*, 178.
(15) Greene-Kelly, R. In *The Differential Thermal Investigation of Clays*; Mackenzie, R. C., Ed.; Mineralogical Society, London, 1957; p140.
(16) Grim, R. E. *Clay Mineralogy*; McGraw-Hill: New York, 1968; pp 313−328, 353−387.
(17) Kingery, W. D.; Bowen, H. K.; Uhlmann, D. R. *Introduction to Ceramics*; Wiley and Sons: New York, 1976; pp 298−315.

resolves the lower temperature event into a two-step process (peak loss rates at 26 and 57 °C) with a third event at 288 °C. This broad temperature regime reflects the numerous environments of water in montmorillonite. Weakly bound, physiabsorbed water and free water pockets within the aggregate structure evolve at the lowest temperatures, where as water within the interlayer and strongly bonded water of hydration (Na^+) evolve at progressively higher temperatures. In contrast, evolution of water and physiabsorbed gases in the OLSs (2044 in this case) is generally complete by 40−60 °C. The water is weakly physiabsorbed or associated with free water pockets within the aggregate structure. Note that although an OLS is conventionally considered hydrophobic because of the addition of alkylammonium cations, water absorption still occurs on the exterior of the aggregates and along the hydrophilic layer edges and depends on environmental conditions, such as relative humidity. In this instance, approximately 1−2 wt % water is contained in the OLS powders. It is interesting to note that this concentration of polar additives has been shown to be sufficient to alter the intercalation response, implying that careful attention to the initial water content of the OLS may be necessary for reproducibility in nanocomposite synthesis.[18]

At temperatures between 200 and 500 °C, the organic constituent in the OLS begins to decompose (Figure 1b). Three overlapping DTG peaks for 2044 indicate that the release of organic substances is staged, arising from different mechanisms. Figure 2 summarizes the DTG curves for the trimethyl alkyl montmorillonites (2044, 2046, 2047, and 2048) and the dimethyl dialkyl montmorillonites (2423, 2428, and 2429). In general, all of the organic-modified montmorillonites decompose in a similar fashion. They exhibit three to four DTG peaks, a lower temperature event resulting in a sharp DTG peak around 200 °C, and two to three closely overlapping higher temperature events producing a broad DTG peak between 300 and 400 °C.

A portion of the MS spectrum of the evolution products from 2044 is shown in Figure 3. Water (m/z = 18), CO_2 (m/z = 44), $NCH_2(CH_3)_2$ (m/z = 58), alkenes (m/z = 55, 69, 83), and alkanes (m/z = 57, 71, 85) are evolved between 200 and 400 °C. C−H vibration at wavenumber 2629, 2853, and 1478 cm^{-1} from TG−FTIR (not shown) further illustrates the release of alkyl and alkene species at these temperatures. Additionally, as with DTG, the MS and FTIR also indicate that the evolution of organic species is staged as indicated by the overlapping peaks between 200 and 400 °C. Furthermore, CO_2 (m/z = 44) evolution indicates that oxidation of residual organic within the OLS begins shortly after general mass loss via alkenes and alkanes ends and before general dehydroxylation of the aluminosilicate begins [evidenced by the observation of H_2O (m/z = 18) from 500 to 900 °C]. Additional experiments on pristine montmorillonite indicate that the abrupt release of CO_2 at 400 °C may also be associated with a small fraction of insoluble metal carbonate impurities. Verification that complete removal of alkyl groups occurs before extensive dehydroxylation is provided by FTIR of pyrolyzed 2044 (Figure 4). After 500 °C anneal,

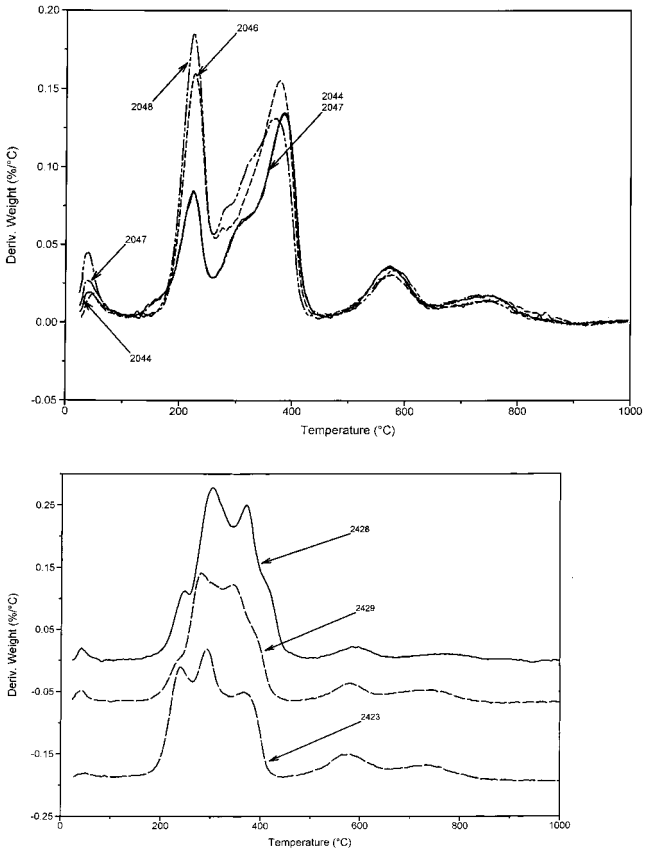

Figure 2. DTG curves from conventional TGA of (a) trimethyl alkyl quaternary ammonium montmorillonites (2044, 2046, 2047, and 2048), and (b) dimethyl dialkyl quaternary ammonium montmorillonites (2423, 2428, and 2429).

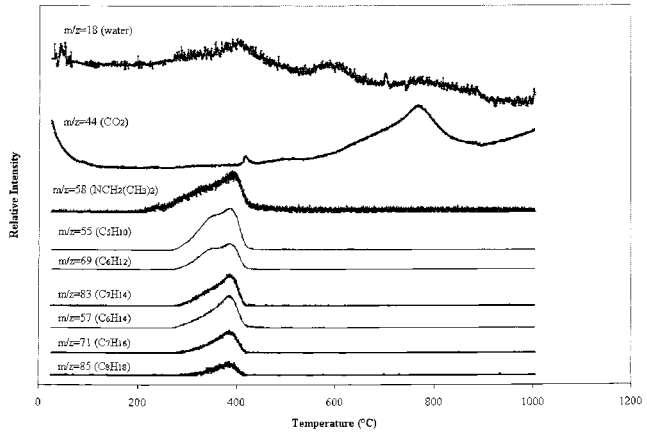

Figure 3. MS results of the evolution products for 2044.

the organic C−H vibrations (wavenumber = 2629, 2853, 1478 cm^{-1}) disappear, while OH vibrations (wavenumber = 3690, 3620, and 1636 cm^{-1})[19,20] remain unchanged in frequency or relative intensity.

From 450 to 700 °C, dehydroxylation of the crystal lattice occurs for Cloisite Na^+. TG−MS results confirm that the major decomposition product for Closite Na^+ is water, corresponding to numerous previous investigations of dehydration reactions in natural montmorillonite and smectites.[21,22] Determination of the break

(18) Burnside, S. D.; Giannelis, E. P. *Chem. Mater.* **1995**, *7*, 1597 1995. Ishida, H.; Campbell, S. *Chem. Mater.* **2000**, *12*, 1260.

(19) Farmer, V. C.; Russell, J. D. *Spectrochim. Acta* **1964**, *20*, 1149.
(20) Miller, G. J. *J. Phys. Chem.* **1961**, *65*, 800.
(21) Koster van Groos, A. F.; Guggenhein, S., *Am. Minerals.* **1984**, *69*, 872−879.

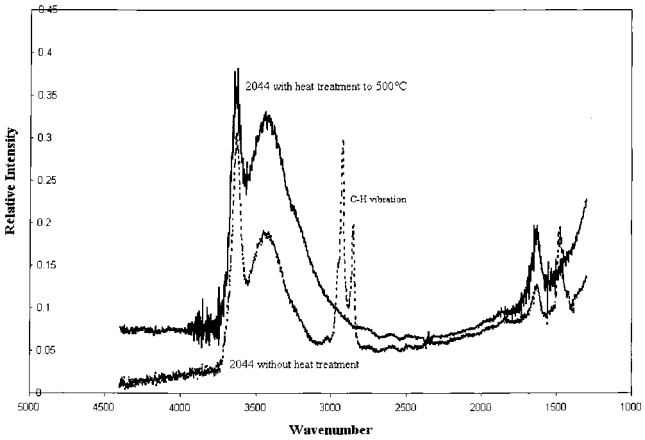

Figure 4. FTIR spectra of 2044 at room temperature and pyrolyzed at 500 °C.

between the evolution of interlayer H_2O and structural −OH, though, is not always straightforward[23] (see, for example, Figure 1a), because molecular water can be bound to fairly high temperatures in defect structures and structural hydroxyl can be released at relatively low temperatures due to these same structural perturbations. HR-DTG spectra reveal a finite break as well as additional detail, indicating that dehydroxylation occurs in three major steps (445, 508, 563 °C), possibly reflecting the local environment of the crystallographic hydroxyls.

For 2044, dehydroxylation and oxidation of the carbonaceous residue occur in two general events between 500 and 1000 °C. As with the Cloisite Na^+, HR-DTA further resolves the mass loss into discrete events, in this instance at least six events. TG−MS (Figure 3) indicates water and CO_2 are evolved at the lower temperatures, implying that carbonaceous residue from the alkyls factors into the dehydroxylation of the crystal lattice. At the higher temperatures, an increased amount of CO_2 is released, beginning around 600 °C and peaking at 800 °C. Metallic species within the aluminosilicate potentially catalyze a reaction between the carbacious residue and the oxygen in the crystal structure of the dehydroxylated montmorillonite, yielding CO_2.[24]

Onset Temperature of Surfactant Degradation. Processing of PLS nanocomposites as well as the initial melt blending of the OLS and polymer normally occur in excess of 150 °C and are near the thermal limits of the organic modifiers. The architecture of the quaternary ammonium ion is nominally chosen to optimize compatibility with a given polymer resin. However, its molecular structure also determines the thermal stability of the OLS. Thermal degradation of the modifier will not only alter the carefully tailored surface compatibility, but also the resulting products may play a major and yet to be determined role in the formation of exfoliated nanostructures or the physical characteristics of the final PLS nanocomposite. Thus, the onset temperature and products of thermal decomposition from 150 to 350 °C are key processing factors to ascertain the degree of chemical and structure change that occurs between room-temperature-characterized OLS and OLS within the final polymer nanocomposite system.

A reproducible procedure to quantify a temperature index for the thermal stability of the OLS and subsequent connection to the parent alkylammonium salt has yet to be developed and generally accepted. Normally, the temperature at a given mass loss or the temperature at the maximum rate of mass loss (peak in DTG) is used. However, overlapping events can introduce large uncertainties in this procedure. Furthermore, the later approach drastically overestimates the onset of chemical changes, since it represents the temperature of greatest mass loss.

Table 3 summarizes various onset temperatures and the temperature at maximum mass loss for the OLSs. As an alternative to the conventional procedures, the onset temperature was also determined as the point where the derivative weight loss is 0.001%/°C over the value of the lower temperature, steady state plateau (heating rate of 2 °C/min in UHP nitrogen atmosphere). As with conventional approaches, low-temperature evolution of small quantities of water and absorbed gases complicates determination of a lower temperature plateau region, increasing the uncertainty in reliably determining the onset of organic decomposition. Thus, after careful analysis of the volatiles by MS, a predrying step within the TGA (140 °C isothermal hold for 60 min, followed by rapid cooling to 60 °C before TGA analysis at 2 °C/min) to remove water and absorbed gases was found to be useful in increasing the reliability of the onset temperature. The precision between experiments using this procedure is approximately ±1.5 °C. In contrast, in the absence of the predrying step, the onset temperatures were unrealistically low (120−140 °C) because of evolution of physiabsorbed water. Note that the use of the temperature at maximum mass loss drastically overestimated the onset and was very sensitive to the heating rate. For example, the maximum mass loss of the initial event for HR-TGA was 25−30 °C lower than conventional TGA (e.g., Figure 1b). However, the onset temperature determined by the deviation of the DTG curve from baseline was comparable ($\Delta T \sim 3-5$ °C) for conventional TGA and HR-TGA.

Alone, TGA is of limited utility, since chemical identification of the volatiles is not possible. Use in conjunction with MS, though, enables direct identification of the release temperature of alkyl degradation products within a background of other gaseous volatiles. The initial fragment of quaternary ammonium degradation was found to be $m/z = 58$ ($NCH_2(CH_3)_2$) and was used as an additional index of the onset of organic decomposition. In general, this onset temperature is approximately 15−20 °C higher than determined by TGA, even though the heating rates in the experiments were identical (2 °C/min). This underscores the general difficulty in using TGA alone to unequivocally identify the onset of degradation within a heterogeneous environment containing various mechanisms that produce or evolve volatiles at comparable temperatures, such as in the aluminosilicates, where the quantity and stability of physioabsorbed water and gas depends on prior process history.

(22) Grim, R. E.; Bradley, W. F. *Am. Miner.* **1948**, *33*, 50−59. Greene-Kelly, R. *Miner. Magn.* **1955**, *30*, 604−615.

(23) Stucki, J. W., Bish, D. L., Duffy, C. J. *CMS workshop lecture, Thermal Analysis in Clay Science.* The Clay Minerals Society, Vol.3, 1990.

(24) Chou, C. C.; McAtee, J. L., Jr. *Clays Clay Miner.* **1969**, *17*, 339−346

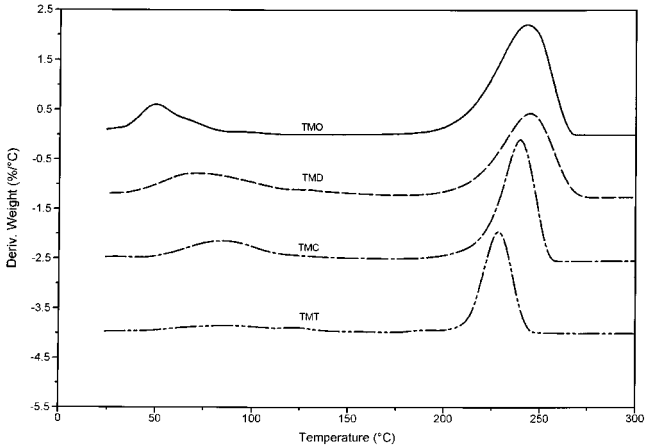

Figure 5. DTG curves from conventional TGA for trimethyl alkyl quaternary ammonium chlorides (TMO, TMD, TMC, and TMT).

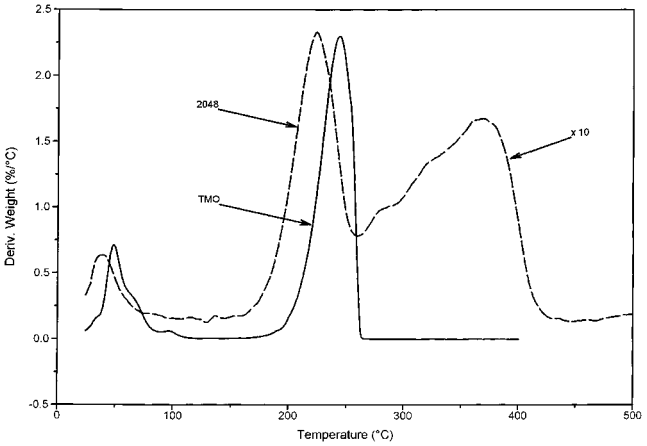

Figure 6. DTG curves comparing pure alkyl quaternary ammonium chloride (TMO) and corresponding OLS (2048).

Table 3 also summarizes temperatures associated with the higher temperature events. The DTG traces generally consist of a sharp peak (used to define T_{max}) superimposed on a broader peak (Figure 2). The relative location of the sharper event with respect to the broader events is sensitive to the heating rate of the experiment (Figure 1b). The lowest derivative weight loss between the first and compound second DTG peaks (as well as the MS traces) was assigned as the onset temperature for these events. There is excellent agreement between MS and TGA results.

Overall, irrespective of architecture (trimethyl or dimethyl), chain length, surfactant mixture, exchanged ratio, or preconditioning (washing), the initial onset temperatures for decomposition of the surfactants within the OLSs are comparable (∼155 °C by DTG and ∼175 °C by TG-MS) with no apparent trends. This conservative estimate (nonisothermal, nonthermal oxidative) is relatively low compared to processing temperatures. Thus, idealized surfactant structures do not persist throughout the OLS and thus the PLS nanocomposite, after temperature excursions approaching 180−200 °C. The extent of alteration to the organic modifiers will depend on the specifics of time−temperature history. However, it cannot be stressed enough that property enhancements of PLS nanocomposites relative to the neat resins are commonly observed, even though they have experienced temperature excursions greater than 180−200 °C in processing and fabrication. Thus, the absolute role of the surfactant to the final PLS nanocomposite properties is not completely understood. Possibly, the property enhancements may even be greater if more stable OLSs were utilized.

As a final point, the overall stability of the surfactant decreases when intercalated into montmorillonite. Figure 5 shows the DTG for the four trimethyl alkyl quaternary ammonium chloride salts used, 2044, 2046, 2047, and 2048, and the various onset temperatures are summarized in Table 3. Overall, mass loss is very similar for these surfactants. Release of water from the surfactant structure (intercalated within the ionic region of the lamallar surfactant salt structure) occurs between 50 and 100 °C. Decomposition of the organic occurs in one event between 200 and 250 °C, roughly corresponding to the lower temperature event in the OLS. Direct comparison of the thermal decomposition events of an OLS (2048) and the corresponding trimethyl alkyl surfactant (TMO) is depicted in Figure 6. The maximum rate of mass loss and onset temperature for these surfactants are consistently 15−25 °C higher than the first events in the OLS. This indicates that the Lewis or Bronsted acid sites in the aluminosilicate have a catalytic effect on the initial stages of decomposition of the organic within the OLS. Additionally, the single-step decomposition of the surfactant salts in contrast to the multistep process of the surfactant within the OLS implies that the presence of the nanoscopic dimensions of the interlayer drastically influences reaction kinetics, product transfer, and volatilization.

Initial Mass Loss of OLS. The initial mass loss event from TGA coincides with the upper temperature environments conventionally encountered by PLS nanocomposite. In contrast to the onset temperature, the fraction of organic evolved during the first event depends on aspects of the OLS, such as surfactant architecture, the MER, and especially the degree of washing. Table 4 summarizes the mass loss associated with different temperature regimes, the total organic mass loss, and the fraction of organic evolved during the initial temperature event. Note that the experimentally determined organic content in the OLSs agrees within a percentage of that anticipated from the MERs (Table 1).

Conditioning the OLS either by Soxhlet extraction (2044a, 2044b, 2044c) or repeated methanol washings (2428a and 2429a) drastically reduces the magnitude of the initial mass loss event. For example, Figure 7 compares the DTG curves for 2044 (trimethyl-coco) washed with ethanol via Soxhlet extraction, showing that the first event continually decreased with increased Soxhlet extraction. At first, it is tempting, especially on the basis of these TGA analyses of the OLS and alkylammonium chloride salts, to speculate that the initial event in OLS decomposition is associated with degradation of the excess surfactant above CEC that resides exterior to the layers. Removal of this surfactant by repeated washings and the corresponding reduction in magnitude of the initial event would then imply that the intercalated surfactants are stabilized by confinement within the interlayer and degrade during the higher temperature events. However, further examina-

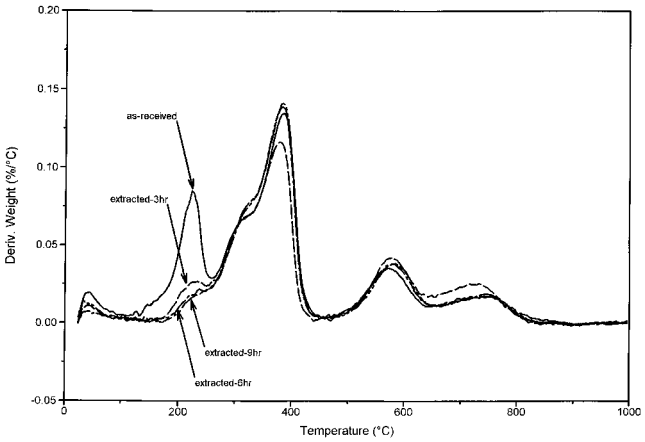

Figure 7. DTG curves for 2044 as-received and after 3, 6, and 9 h of Soxhlet extraction with ethanol.

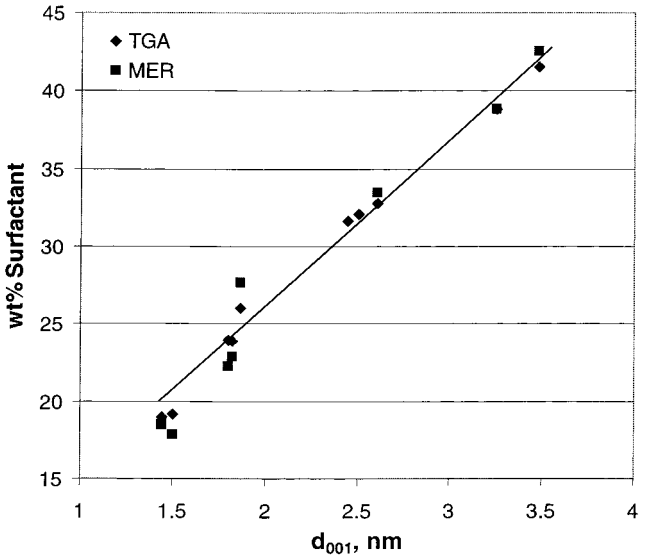

Figure 8. Comparison of the total organic content experimentally determined from TGA and predicted from MER with regards to the interlayer spacing determined from X-ray diffraction.

tion of the results indicates this initial hypothesis is not correct.

Comparison of layer repeat distance and total organic content indicates that the majority of the excess surfactant in these systems (i.e., equivalence of surfactant greater than the cation exchange capacity of the montmorillonite) is contained within the interlayer—not physioabsorbed to the exterior of the crystallites or contained in voids within the OLS aggregate structure. Figure 8 compares the interlayer spacing (X-ray diffraction) to the total organic content experimentally determined from TGA and predicted from MER. The linear correlation indicates that the majority of the excess surfactant resides within the interlayer, irrespective of architecture or degree of washing.[25] Thus for these preparation procedures, overexchanged montmorillonites do not have a substantially greater fraction of surfactant residing outside the interlayer than do montmorillonites exchanged at equivalence. The surfactant molecules reside in the confined interlayer environment whether directly associated to the aluminosilicate or a chloride anion.

Overall, the fraction of organic released during the initial event is strongly correlated to initial interlayer spacing and surfactant architecture (Tables 1 and 4). For a given surfactant architecture, the initial fraction of organic evolved decreases with the interlayer spacing of the OLSs. For example, interlayer spacing decreases with decreasing MER (2427, 2428, 2429), shorter alkyls (2048 and 2047; 2046 and 2044), or removal of surfactant in excess of the CEC [methanol washing of 2428 (d_{001} = 3.25) yielding 2428a (d_{001} = 2.50)]. These correspond to a lower fraction of mass evolved in the first event. Additionally, a smaller fraction of mass is evolved from OLSs containing dimethyl than trimethyl surfactants (e.g., 2429 and 2046). Note that dimethyl OLSs generally have larger interlayer spacings than trimethyl OLSs, but a smaller fraction of organic is evolved from the former in the initial event.

This overall behavior is consistent with the nanoscopic dimensions of the interlayer altering product transfer, product concentration, and thus the efficiency of secondary reactions, but not necessarily the chemical stability of the intercalates. A smaller gallery height is expected to retard the rate of volatile evolution of the long chain decomposition products and thus decrease the fraction of mass detected in the first event. The larger number of long alkyl chains in the interlayer for dimethyl relative to trimethyl surfactants will result in a larger fraction of higher molecular weight products within the interlayer upon decomposition. This will also decrease the mean interlayer mobility, decreasing the rate of volatile release and detection, even though the interlayer spacing is larger. This picture is consistent with the similarity of onset temperatures irrespective of surfactant architecture, initial MER, or degree of washing. Thus, a detailed understanding of the morphology of the aluminosilicate and the decomposition products is critical in understanding the decomposition process of OLSs.

TGA and related techniques preferentially reflect decomposition events that produce volatiles. If the material structure, such as a thermally stable stacking of plates and associated nanoscale lamellar slits, inhibits or alters the rate of release of volatiles, thermal decomposition events and detection of escaped volatiles do not necessarily have to coincide. Thus, the role of morphology and the decomposition products themselves need to be carefully examined in considering the implications of the initial mass loss event in the OLSs.

Structural Changes During OLS Decomposition. Alkyl salts are lamellar ionic crystals comprised of alternating layers of paraffinic alkyl chains and of ionic groups and associated water of hydration. Upon degradation around 200 °C, the entire structure is rapidly and completely destroyed. In contrast, the layered morphology of the aluminosilicate persists throughout the surfactant decomposition event, kinetically (and catalytically) altering the reaction pathway.

In situ X-ray diffraction of the decomposition process yielding the layer repeat distance (d_{001}) and the fwhm of the basal reflection is summarized in Figure 9 for 2427 and 2429. The fwhm is inversely proportional to

(25) Linear relation between interlayer height and surfactant content is consistent with previous investigation of OLS with long chain quaternary alkyl surfactants.[11] Staging only occurs for shorter alkyl chains and lower interlayer surfactant densities.[26]

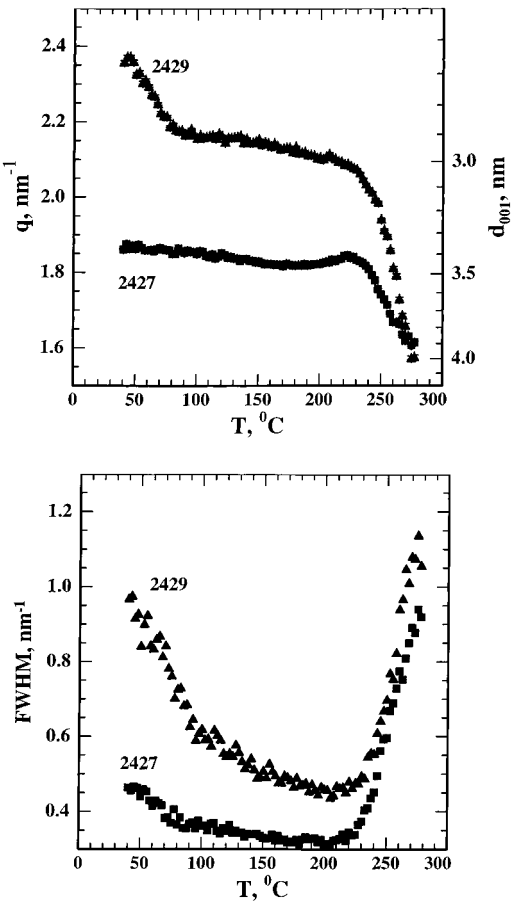

Figure 9. Summary of results from in situ small angle scattering of degradation (5 °C/min) of 2427 and 2429: (a) position of basal reflection (d_{001}) and (b) fwhm of basal reflection.

the extent of layer registry through the Scherrer equation.[27] These dimethyl dihydrogenated tallow montmorillonites exhibit the same decomposition processes as previously discussed and differ only in the amount of surfactant present in the structure (MER = 140 for 2427 and 95 for 2429). The majority of the excess surfactant resides in the interlayer (larger layer repeat distance, d_{001}) and results in a larger initial weight loss (Table 4).

The initial increase in layer repeat distance (d_{001}) and layer registry (≈fwhm^{-1}) from 50 to 100 °C is due to melting of the intercalated surfactant, which creates a fluidlike environment between the layers, enabling local relaxation of residual stress and packing imperfections associated with prior process history. This behavior agrees with previous observations of other alkylammonium smectites.[11,28] The slight increase in d_{001} from 100 to 200 °C is attributed to the thermal expansion of the structure normal to the layers. From 200 to 280 °C, an increase in d_{001} and a decrease in layer registry (increase in fwhm) accompany the first OLS degradation event. These changes in the organization of the aluminosilicate layers reflect the production of volatiles and the associated increase of internal pressure within the interlayer, leading to the expansion of the structure, layer disorder, and potentially defect generation. This verifies that the initial decomposition event is not restricted to unconfined surfactant (i.e., external to the interlayer), but also includes intercalated, confined surfactant.

Note that the in situ observation that gallery height increases with decomposition contrasts previous studies that indicate that the gallery height decreases after decomposition. For example, previous studies of the structure of surface char on combusted nanocomposites revealed a collapse of layer spacing upon thermal decomposition of the hybrid structure.[29] Taken together these studies indicate that the organization of the aluminosilicate layers appears to initially disorder during thermal decomposition and, depending on the decomposition route and temperature, collapse to varying degrees after completion of volatile release. Thus, utilization of interlayer decomposition and production of volatiles to increase interlayer pressure, effectively increasing layer separation by gaseous expansion, provides a new, although unproven, paradigm for surfactant design for enhancing exfoliation in melt-processed polymer nanocomposites.

Degradation Products. A list of products determined by pyrolysis/GC−MS from 2048 during the first and second thermal events and from TMO is summarized in Table 5. These are generally representative of the products from the other trimethyl alkyl OLSs and ammonium salts.

Degradation of TMO yields long chain tertiary amines, long chain α-olefins, and 1-chloroalkanes. GC−MS at the beginning (200 °C), maximum mass loss (250 °C), and completion (300 °C) of the decomposition process indicated that the same type of fragments (tertiary amines, α-olefins, and 1-chloroalkanes) are presented throughout, with an increased number of shorter chain fragments at the higher temperatures. Decomposition of ammonium salts generally proceeds either by a Hoffmann elimination reaction or an S_N2 nucleophilic substitution reaction. Hoffmann elimination occurs in the presence of a basic anion, such as hydroxide, which extracts hydrogen from a β-carbon of the quaternary ammonium, yielding an olefinic and tertiary amino group.[30] Nucleophilic attack at elevated temperatures of the chloride on R_4N^+ favors the reverse of the quaternary ammonium synthesis, yielding RCl and R_3N. For neat TMO, the later is probably favored, although a fraction of olefins is detected.

For the OLS, the proximity of the Lewis base sites and the basic aluminosilicate surface to the intercalated alkyl quaternary ammonium molecule is conducive to enhancing (lowering the energy of) the Hoffmann elimi-

(26) Lagaly, G.; Beneke, K.; Weiss, A. *Am. Mineral* **1975**, *60*, 642. Beneke, K.; Lagaly, G. *Am. Miner.* **1997**, *62*, 763. Beneke, K.; Lagaly, G.; *Am. Miner.* **1983**, *68*, 818. Lagaly, G. *Philos. Trans R. Soc. London A* **1984**, *311*, 315.

(27) The Scherrer equation relates the crystallite or tactoid size, l, to the full-width at half maximum of the basal reflection, *b*, as $l = \kappa\lambda/(\beta \cos \theta)$ where λ is the wavelength of radiation, θ is half the diffraction angle, and *k* is a constant, ~0.94 for *b* in degrees. Basal reflections will provide a measure of the extent of coherent stacking normal to the silicate layers. Warren, B. E. *X-ray Diffraction*; Dover Publications: New York, 1990.

(28) Wang, L.-Q.; Liu, J.; Exarhos, G. J.; Flanigan, K. Y.; Bordia, R. *J. Phys. Chem. B* **2000**, *104*, 2810. Hackett, E. Manias, E. Giannelis, E. P. *Chem. Mater.* **2000**, *12*, 2161.

(29) Gilman, J. W. *Appl. Clay Sci.* **1999**, *15*, 31−49.

(30) Cope, A. C.; Trumbull, E. R. In *Organic Reactions 11*; John Wiley and Sons: New York, 1960; pp 317−487. March, J. *Advanced Organic Chemistry, Reactions, Mechanisms and Structures*, 4 ed.; John Wiley and Sons: New York, 1992; pp 982, 999−1001.

Table 5. Representative Organic Species Evolved from 2048 and TMO (pyrolysis/GC−MS)

	200 °C	400 °C
	2048	
alkane, linear 1-chloro	$C_{16}H_{33}Cl$, $C_{18}H_{37}Cl$	
branched alkane	tridecane, 3-methyl-, $C_{14}H_{30}$	
tertiary amine, *N*,*N*-dimethyl-	$C_{15}H_{33}N$, $C_{17}H_{37}N$	$C_{15}H_{33}N$, $C_{17}H_{37}N$
primary amine, linear		$C_{18}H_{39}N$
linear alkene, 1-	$C_{16}H_{32}$, $C_{17}H_{34}$	C_9H_{18}, $C_{10}H_{20}$, $C_{14}H_{26}$, $C_{17}H_{34}$
linear alkene, *n*-		3-nonene, (*E*)-[C_9H_{18}]; 2-decene, (*Z*)-[$C_{10}H_{20}$]; 3-undecene, (*E*)-[$C_{11}H_{22}$]; 5-dodecene, (*Z*)-[$C_{12}H_{24}$]; 3-tridecene, (*Z*)-[$C_{13}H_{26}$]; 6-tridecene, [$C_{13}H_{26}$]; 3-octadecene, (*E*)-[$C_{18}H_{36}$]; 3-octadecene, (*E*)-[$C_{18}H_{36}$]
branched alkene		1-octene-3-methyl-, [C_9H_{18}]; 3-heptene-2,6-dimethyl-, [C_9H_{18}]; 4-nonene-2-methyl-, [$C_{10}H_{20}$]; 1-octene-3,7-dimethyl-, [$C_{10}H_{20}$]; 4-undecene-10-methyl-, (*E*)-[$C_{12}H_{24}$]
linear aldyhyde		$C_{14}H_{28}O$, $C_{15}H_{30}O$, $C_{16}H_{32}O$
branched aldhyde		(*E*)-15-hepadecenal, [$C_{17}H_{32}O$]
	TMO	
alkane, linear 1-chloro	$C_{13}H_{29}Cl$, $C_{16}H_{33}Cl$, $C_{18}H_{37}Cl$	
tertiary amine, ***N***,*N*-dimethyl-	$C_9H_{21}N$, $C_{10}H_{23}N$, $C_{15}H_{33}N$, $C_{17}H_{37}N$	
linear alkene, 1-	$C_{10}H_{20}$, $C_{12}H_{24}$	

nation reaction, as seen by the lower onset temperature for the OLS and increased olefinic production. 2048 contains unexchanged surfactant, as verified by the presence of 1-chloroalkanes in the degradation products. The additional presence of branched alkanes implies that auxiliary secondary reactions, such as olefinic addition, occur between products within the OLS, complicating a simple explanation of product generation based on the current observations.

During the higher temperature decomposition events of 2048, long chain tertiary amines are observed along with shorter chain olefins, branched olefins, and aldhydes. Confined within montmorillonite's lamallar crystal structure, the initial products undergo successive secondary reactions such as alkyl chain scission, free-radical condensation, and additions to olefinic groups. The presence of oxygen and metal species in the montmorillonite structure may serve as catalysts to enable the oxidative cleavage of alkenes to produce aldehydes at elevated temperature. Kinetic analysis of TGA results[30] from the trimethyl alkyl montmorillonites indicated that the activation energy for the second series of events is 50−100 kJ/mol higher than the first event (156−162 kJ/mol),[31] mirroring the GC−MS results.

Discussion

The decreased stability, different decomposition products, and accompanying higher temperature events observed during OLS decomposition attest to the major role of the aluminosilicate chemistry and morphology in the thermal decomposition process of the organic intercalates.

Thermal decomposition of organic molecules predominately occurs at the site with the smallest bond dissociation energy. The bond energies within alkylamines generally (with regard to the various possible substituents) decrease in the order C−H (96−99 kcal/mol), N−H (93 kcal/mol), C−C (83−85 kcal/mol), and C−N (69−75 kcal/mol).[32] Formation of the ammonium will weaken the C−N bond by increasing the effective electronegativity of the nitrogen. For example, this is reflected in a longer C−N bond for $(CH_3)_4N^+$ (1.493 Å) relative to $(CH_3)_3N$ (1.445 Å) (semiempirical AM1, HyperChem v 5.1). This corresponds experimentally to the initial evolution of $NCH_2(CH_3)_2$ (Figure 3) from the decomposition of the trimethyl alkylammonium salts and the associated montmorillonite.

Hindrance of molecular reorientation and mass transport within the nanoscopic interlayer will alter reaction kinetics and increase the transient concentration of products. These effects will enable alternative reaction pathways, secondary reactions, and radical termination by the aluminosilicate surface and possibly increase the propensity for reverse reactions. Nyden and co-workers observed similar confinement effects on decomposition reactions within a slit using molecular dynamic simulations.[33] The fundamental stability of the C−N linkage, though, will be determined less by the nanoscopic environment than by the local kinetic energy (reflected by the temperature), presence of catalytic species, and local concentration of coreactants (such as O_2). The oxidative stability of a molecule may increase due to the role of confining morphology in modifying oxygen transport, but for the nonoxidative decomposition examined here, there is no reason a priori to suspect that localization of the surfactant within the interlayer will increase the thermal stability. For example, XRD indicates that structural (and by inference chemical) changes occur within the interlayer during the first event. In actuality, the decrease in onset temperature of the OLSs relative to the ammonium salts indicates that catalytic sites on the aluminosilicate surface (whether at the layer edge or on the siloxane surface) decrease the stability of surfactant in close proximity to these sites.

Since the local environment does not increase the energetic stability of the alkylammonium, the elevated temperature events and the relative amount of mass loss during the initial decomposition event must reflect

(31) *Standard Test Method for Decomposition Kinetics by Thermogravimetry*, ASTM E1641-99, Annual Book of ASTM Standards, March 2000.

(32) March, J. *Advanced Organic Chemistry: Reactions Mechanisms and Structure*, 4th ed.; Wiley: New York, 1992; p 24.

(33) Nyden, M. R.; Gilman, J. W. *Comput. Theor. Polym. Sci.* **1997**, *7*, 191.

the influence of the aluminosilicate structure on the reaction kinetics and the mobility of decomposition products. Overall then, a picture emerges as to the thermal−chemical events in the OLS and near the aluminosilicate surface as observed by analysis of volatile products.

Initial decomposition of the surfactant via Hoffmann elimination or nucleophilic substitution reaction occurs within and exterior to the interlayers at temperatures comparable to (or less than) the pristine quaternary ammonium salt. The mass evolution occurring in the initial event originates from "unconfined" surfactants, whether associated with the layers or small molecule anions. These unconfined surfactants reside outside of the interlayers, such as those complexed to the exterior of the crystallites or within void spaces and inside the interalyers but within proximity of the terminus of the gallery. The onset observed will be directly related to the thermal stability of the surfactant and the catalytic influence of the aluminosilicate. The relative magnitude of the observed mass loss will depend on factors effecting mass transfer of the products, such as defect concentration, perfection of layer stacking, crystallite size, and packing density of the aggregate. These factors, with the exception of layer size, are dependent on the process history of the OLS.[34] Furthermore, this implies that future examination of the initial decomposition process within the interlayers will require solid-state characterization techniques, such as in situ, elevated temperature FTIR of the solid, rather than analysis of the volatile product stream.

As the temperature increases, the higher molecular weight products that are trapped within the interlayers undergo further reactions (C−C scission, oxidation, and dehydrogenation), radical cross-linking, or cyclization reactions. On average, increased temperature will favor production and increased evolution of smaller molecular weight species and thus the additional higher temperature DTG peaks and associated lower molecular weight species in the mass spectrum and pyrolysis/GC results. Occurrence of these higher energy processes is further verified by the increased activation energy associated with mass evolution during these later events. On the whole, these processes parallel those observed in petroleum cracking using MCMs and pillared clays.[35,36]

The implication of these conclusions to determining the thermal stability of OLSs in exfoliated PLS nanocomposites warrants comment. As previously mentioned, the magnitude of the initial mass loss detected by TGA reflects more the condition of the OLS crystallite structure than any chemical enhancement of thermal stability. Since an exfoliated OLS does not possess morphological features associated with the inorganic lamallar stack that would confine product transport, the nonoxidative thermal stability of the surfactants will at best be comparable to the stability of the parent surfactant if catalytic effects of the aluminosilicate are minimal. Along similar lines, the molecular species produced by degradation is expected to parallel that of the parent surfactant. Since the products observed during the higher temperature degradation events are related to retardation of degradation products and subsequent secondary reactions among products, they are not anticipated to be present in exfoliated PLS nanocomposites. Overall, the presence of long chain alkane and alkene products from the decomposition of the surfactant may lead to detrimental interfacial plasticization or advantageous secondary cross-linking reactions (1-olefins and associated radicals) with the polymer. Determination of the importance of these factors on the interfacial strength between polymer and silicate and subsequent impact on mechanical properties requires additional investigation.

Finally, verification that surfactant decomposition can occur at relatively low temperatures with respect to those conventionally used in melt processing implies that the interfacial energetics between the OLS and an intercalating polymer may be drastically different, and more complex, than originally intended by selection of the organic modifier for the OLS. Additionally, the production of nontethered, long chain molecules and of radical species that can form cross-links increases the complexity of determining chain dynamics near the OLS surface and molecular interpretation of rheological phenominum. Further investigation is crucial to clarifying the role (advantageous or detrimental) of these small molecular products in the fundamental thermodynamic and kinetic aspects of polymer melt intercalation.

Conclusion

In summary, the nonoxidative thermal degradation of montmorillonite and quaternary alkylammonium-modified montmorillonite were examined using conventional and high-resolution TGA combined with TG−FTIR−MS and pyrolysis/GC−MS. The onset temperature of decomposition of these OLSs was approximately 155 °C via TGA and 180 °C via TGA−MS, where the TGA−MS results enable the differentiation of water desorbtion from true organic decomposition. Analysis of products (GC−MS) indicates that the initial degradation of the surfactant in the OLS follows a Hoffmann elimination reaction and that the architecture (trimethyl or dimethyl), chain length, surfactant mixture, exchanged ratio, or preconditioning (washing) does not alter the initial onset temperatures. However, these factors do effect the initial mass loss. Relative to the parent alkyl quaternary ammonium salt, catalytic sites on the aluminosilicate layer reduce the thermal stability of a fraction of the surfactants by an average of 15−25 °C. Finally, the release of organic compounds from organically modified montmorillonite is staged and is associated with retardation of product transfer arising from the morphology of the OLS. These studies provide the foundation for a subsequent investigation of the influences of the various inorganic (e.g. mineral, isomorphic substitution, crystal habit, layer charge density) and organic (surfactant architecture, chemical composition, omium type, covalent attachment) factors on the thermal−oxidative stability of the OLS and PLS nanocomposites.

(34) Washing of the OLS not only removes unexchanged surfactant but increases the perfection of the layer stacking, as indicated by the decrease in the fwhm and perfection of the Gaussian shape of the basal reflection. Similar perfection of the layer stacking occurs for thermal anneals above the melting point of the intercalated surfactants (Figure 9).

(35) Ward, J. W. *Fuel Processing Technol.* **1993**, *35*, 55−85.

(36) Hagg, W. O. In *Zeolites and Related Microporous Materials: State of the Art 1994*; Weitkamp, J., Ed.; Elsevier. Amsterdam, 1994; Vol 84 (PA-C), pp 1375−1394.

Finally, recall that property enhancements of PLS nanocomposites using quaternary alkyl surfactants are commonly observed. Additionally, polymer melt intercalation occurring in excess of 180−200 °C is generally reported. The verification that chemical degradation occurs for the alkylammonium surfactants around 180 °C does not imply that these OLSs are not useful in the formation of PLS nanocomposites. What is implied is the general understanding of PLS nanocomposites and the factors that lead to formation and enhanced properties may not be completely rationalized.

Acknowledgment. The authors are grateful to L-S. Tan for detailed technical discussions. The Air Force Office of Science Research (F49620-00-1-0260) and the Air Force Research Laboratory, Materials and Manufacturing Directorate provided financial support.

CM010305S